Journal of Applied Pharmaceutical Research
Volume 14 Issue 3, Year of Publication 2026, Page 155 – 176
DOI: https://doi.org/10.69857/joapr.v14i3.2063

Check for updates

Research Article

JOURNAL OF APPLIED PHARMACEUTICAL RESEARCH | JOAPR
www.japtronline.com ***ISSN: 2348 – 0335***

DESIGN AND CHARACTERIZATION OF A MUCOADHESIVE NANOPARTICLE-LOADED THERMO-RESPONSIVE IN-SITU NASAL GEL FOR ENHANCED BRAIN DELIVERY OF AN ANTIMIGRAINE DRUG

Mansi Butola[1*], Vikash Jakhmola[2]

Article Information
Received: 15th January 2026
Revised: 9th April 2026
Accepted: 28th April 2026
Published: 15th May 2026

Keywords
Antimigraine, Blood-brain barrier, Central nervous system, Patient adherence, Nasal integrity.

ABSTRACT
Background: Migraine is a debilitating neurological disorder that requires rapid and effective drug delivery to the brain. Conventional oral and parenteral therapies are associated with delayed onset of action, low patient compliance, limited central nervous system (CNS) bioavailability due to the blood-brain barrier (BBB), and hepatic first-pass metabolism. This study aimed to develop a thermoresponsive, mucoadhesive, nanoparticle-loaded nasal in situ gel to enhance brain delivery of an antimigraine drug. **Methodology:** Drug-loaded nanoparticles were prepared via ionic gelation and incorporated into a thermo-sensitive nasal in situ gel via the cold method. **Results and Discussion:** The optimized nanoparticle formulation (NP13) exhibited a small particle size (154.3 nm), acceptable polydispersity index (0.3485), positive zeta potential (22.79 mV), high entrapment efficiency (89.09%), drug loading (14.33%), and sustained drug release (90.26%). The developed in situ gel showed optimal pH (6.8), suitable gelling temperature (28–34 °C), viscosity (556 cp), entrapment efficiency (85%), drug content (95.82%), in vitro drug release (88.89 ± 0.98%), and ex vivo permeation (85.24 ± 0.67%) over 10 hours. Histopathological studies confirmed minimal nasal mucosal irritation compared to the drug solution and isopropyl alcohol. MTT assay results demonstrated concentration-dependent cytotoxicity, with SS-NPs ISG4 showing higher cell viability than the free drug, indicating reduced cytotoxicity due to nanoparticle encapsulation. Blank nanoparticles exhibited maximum cell survival, confirming carrier biocompatibility. **Conclusion:** The developed nanoparticle-loaded nasal in situ gel demonstrated promising safety, biocompatibility, and enhanced delivery potential, validating its suitability for intranasal migraine therapy.

INTRODUCTION

Migraines are intensely painful, recurring episodes that affect the nervous system. Approximately 15% of the global population has been affected by this chronic neurological disorder. Individuals with migraine suffer severe and

[1]*Department of Pharmaceutics, Uttaranchal Institute of Pharmaceutical Sciences, Uttaranchal University, Dehradun, Uttarakhand, India, 248007.*
[2]*Department of Pharmaceutical Chemistry, Uttaranchal Institute of Pharmaceutical Sciences, Uttaranchal University, Dehradun, Uttarakhand, India, 248007.*

For Correspondence: **mansibutola1995@gmail.com**

debilitating health issues. It appears with recurring, unilateral, pulsating headache episodes that vary in intensity from mild to severe. Headache is the second most frequent cause of migraines, with other prominent symptoms including nausea, vomiting, photophobia, and/or phonophobia. The symptoms might get worse progressively. The migraine discomfort reached its maximum intensity after 2–12 hours and then gradually decreased. However, it appears to be an attack if it lasts 4 to 72 hours [1]. Although the precise pathophysiology of migraine remains unidentified, it is widely acknowledged that migraine results from the activation and sensitization of trigeminal nerve fibers due to neurogenic inflammation. Trigeminal neurons possess a single axon that splits into central and peripheral branches, both of which can stimulate them. Various migraine triggers exist, including physiological, nutritional, and environmental variables that activate the trigeminal nerve fibers, potentially leading to migraine episodes [2,3]. The physiological conditions associated with trigeminovascular activation offer potential for novel antimigraine drugs and facilitate in vivo studies into the molecular origins of cephalic pain. Therefore, drugs with rapid pharmacological effects are often used to restore the patient's functional abilities [4,5] quickly.

The existing treatments for migraines are predominantly non-specific and characterized by low patient compliance. The effective treatments for acute migraine include nonsteroidal anti-inflammatory drugs (NSAIDs), ergot alkaloids, and triptans (serotonin hydroxytryptamine (5-HT) 1B/1D receptor agonists) [5]. Triptans are specific antimigraine drugs that can successfully reduce migraine discomfort. Triptans have been used as a primary treatment for moderate to severe migraine headaches. However, using them can often be restricted due to adverse reactions, time and frequency restrictions, and the potential for developing drug-overuse headaches [2]. Sumatriptan succinate (SS), the most often prescribed drug, garnered approval from the US FDA for migraine attacks in 1992. The SS administration shows the most potent antiemetic properties, which may reduce migraine-associated nausea. The safety and efficacy of many administration routes of ST (e.g., oral, intranasal, transdermal, subcutaneous, and rectal) have been examined in numerous clinical trials, and corresponding formulations are being used [6]. Intranasal medication delivery has potential and is a successful technique. Nasal administration has many benefits, including localized distribution, brain targeting, systemic drug delivery, avoidance of first-pass metabolism, ease of use, and improved patient compliance. Despite this, there are several problems with intranasal medication delivery [7]. For instance, mucociliary clearance (MCC), a defensive mechanism that eliminates foreign material in 15 to 20 minutes, is very difficult to overcome; nasal passageways are inhaled with restricted permeability, the pH is generally low, and the amount of dosage provided is little [8]. To guarantee that drugs are more effective and that their effects last, the design approach should be considered. Numerous studies have demonstrated that nanoparticles can hold a formulation in the nasal cavity, delaying nasal MCC's quick removal [9]. When nanoparticles are added to an in-situ gelling polymer that responds to stimuli, the active ingredients are also released. Since nasal administration has been used for hundreds of years, it is a good way to provide medication [10].

It is thought to be a major aid in the treatment of numerous neurological conditions and to facilitate the delivery of many medications to the brain. The nose is crucial because it receives the ophthalmic and maxillary divisions of the trigeminal nerve, has specific ciliated nerve cells that aid in smell, and provides direct access to cerebrospinal fluid. The intranasal approach uses the olfactory and trigeminal nerves to deliver medications to the brain. Drug administration to the brain via the nasal route is considered non-invasive. It can overcome the problems with the oral route, such as first-pass metabolism and the challenging BBB [4]. Furthermore, the intranasal route has been linked to the quick action and high brain concentration of the medication needed to treat acute migraines. Although the intranasal route has certain benefits, the main drawbacks are that the formulation would be rapidly eliminated from the body via mucociliary clearance and that the residence time and enzymatic degradation would be shortened. Mucoadhesive nano-vesicular carriers solve these problems by making it easier for medications to remain on the nasal mucosa, be absorbed by cells & move within cells. In addition to being resistant to enzymatic degradation, they may also make medications more accessible in different parts of the brain [3]. In the last three decades, there has been a growing focus on the development of strictly controlled and sustained drug delivery systems. Significant research initiatives have focused on the development of polymer-based systems, including in situ gels [11]. These systems have attracted much attention recently. They initially appear as liquid aqueous solutions and transition into gels under physiological conditions. The ability to maintain a constant drug release rate, combined

with biocompatibility, stability, and reliable drug levels, improves accuracy [12]. Among the CS-based nanocomposites, nanoparticles (NPs) produced via ionotropic gelation are the most thoroughly studied.

The procedure involves sol-gel transition of chitosan polymers prompted by their contact with a poly-anionic crosslinking agent, commonly STPP [13]. Among the nanoparticles synthesized from biodegradable polymers, chitosan-based nanoparticles are among the most promising delivery systems for the treatment and diagnosis of brain diseases due to their distinctive properties. CS has primary amine groups on the glucosamine residues at the C2 position, imparting essential properties that are suitable for bio-fabrication into nanoparticles. Research has shown that CS possesses unique mucoadhesive characteristics, allowing prolonged adhesion to the nasal mucosa and improving drug absorption [14,15]. This adhesion restricts mucociliary clearance, thereby prolonging drug contact. Furthermore, the cationic properties of chitosan facilitate paracellular transportation by temporarily disrupting tight junctions between epithelial cells [16]. This method enhances the permeability of the nasal epithelium, therefore improving drug absorption efficiency. Carbopol is a pH-sensitive polymer used for gel formulation at nasal pH, which appears to enhance drug release and direct intranasal delivery of drugs [11,17].

This study aims to develop and assess SS-loaded chitosan nanoparticles (CS-NPs) within an in situ gel, designed for migraine treatment via a non-invasive intranasal route, enabling direct drug delivery from the nasal cavity to the brain. The formulation procedure involves optimizing the CS-to-STPP ratio to achieve effective drug loading using a Box-Behnken statistical design (BBD). After optimization, the SS-loaded CS-NPs were incorporated into a temperature-sensitive carbopol gel to prepare an in situ gel containing SS-loaded CS-NPs, which was subjected to comprehensive physicochemical evaluation. The research further includes in vitro drug release, ex vivo permeability, histopathology, MTT analysis, and stability studies.

MATERIALS AND METHODS

Materials

Intas Pharmaceuticals Ltd. sent us a free sample of Sumatriptan Succinate (SS), Central Drug House Pvt. Ltd. sold us Poloxamer 188 and 407, Carbopol 934, Chitosan (CS), and Sodium Tripolyphosphate (STPP).

Methods

Pre-formulation Studies

Solubility Profile

After dissolving an excess of the medication in a solvent, the mixture was shaken for 3 hours at 70–80 RPM in a rotary flask shaker. After reaching saturation, the solution was filtered, diluted, and analyzed at the specified wavelength (nm). Three duplicates of the experiment were carried out.

$$\boldsymbol{Solubility} = \frac{\boldsymbol{Concentration} \times \boldsymbol{Dilution\ factor}}{\mathbf{1000}}$$

Experimental design for Cs-NPs

To optimize sumatriptan succinate nanoparticles and assess primary, quadratic, and interaction effects on entrapment efficiency, drug loading percentage, and drug release percentage, the Box-Behnken statistical design (BBD) was selected. A second-order polynomial equation was derived using a three-factor, two-level BBD[18]. Using Design-Expert software (version 11, Stat-Ease Inc., Minneapolis, Minnesota), the response surface methodology (RSM) employed the BBD and included 17 confirmatory formulation runs, including five center points. As indicated in Table 1, EE, DL, and DR were selected as dependent factors, and chitosan (CS), poloxamer, and sodium tripolyphosphate (STPP) were selected as independent variables.

To reduce experimental variability and increase the accuracy of the model's predictions, the trials were conducted in a random order[19]. To display the polynomial equations created for each answer, we created three-dimensional response surface graphs. This demonstrated the relationship between the independent and dependent variables.

Regression analysis, including evaluation of regression coefficients, the coefficient of determination (R^2), and lack-of-fit tests, was used to examine the accuracy and dependability of the experimental data. The expected value of R can be predicted using the equation of the non-linear quadratic model shown below [20,21].

$$R=\beta_0+\beta_1A+\beta_2B+\beta_3C$$
$$+\beta_{12}AB+\beta_{13}AC+\beta_{23}BC+\beta_{11}A^2+\beta_{22}B^2+\beta_{33}C^2$$

Where,

R = Response Variable

A, B, and C = Independent Variables

β_0, β_1, and β_3 are the coefficient estimates by the design expert

Table 1: Variables and their limit with responses

Variables	Levels	
	Low (-1)	High (+1)
	Independent Variables	
1. Chitosan(mg)	0.1	1
2. Poloxamer (mg)	0.5	1.5
3. STPP (mg)	0.1	2
	Dependent Variables	
R1; Entrapment Efficiency EE%	Maximum	
R2; Drug Loading DL %	Maximum	
R3; Drug Release DR %	Maximum	

Method of Preparation of Sumatriptan Succinate Nanoparticles (SS-NPs)

Ionic gelation method was used to prepare Chitosan (molecular weight (100–300 kDa) and degree of deacetylation (DDA) 75–90%) nanoparticles loaded with SS. First, several quantities of chitosan were dissolved in a 2% aqueous acetic acid solution. To guarantee thorough mixing, the chitosan solutions were agitated at room temperature at 200 rpm. Stirring constantly, add poloxamer 188 to the chitosan solution. Poloxamer 188 helps stabilize nanoparticles and improve their mucoadhesive or thermosensitive qualities [13]. Five milliliters of the chitosan poloxamer solution were used to dissolve the appropriate amounts of SS.

Then, using a 0.5 mL syringe and magnetic stirring at 500 rpm, 2 mL of a 0.3% w/v aqueous STPP solution was added to the CS solution. To ensure complete interaction between CS and STPP for optimal cross-linking, the resulting nanoparticle dispersion was sonicated for 7–10 minutes using a probe sonicator. Nanoparticles spontaneously form due to ionic interactions between the negatively charged STPP and the positively charged chitosan. As seen in Figure 1, the produced nanoparticles were then dried and gathered [22].

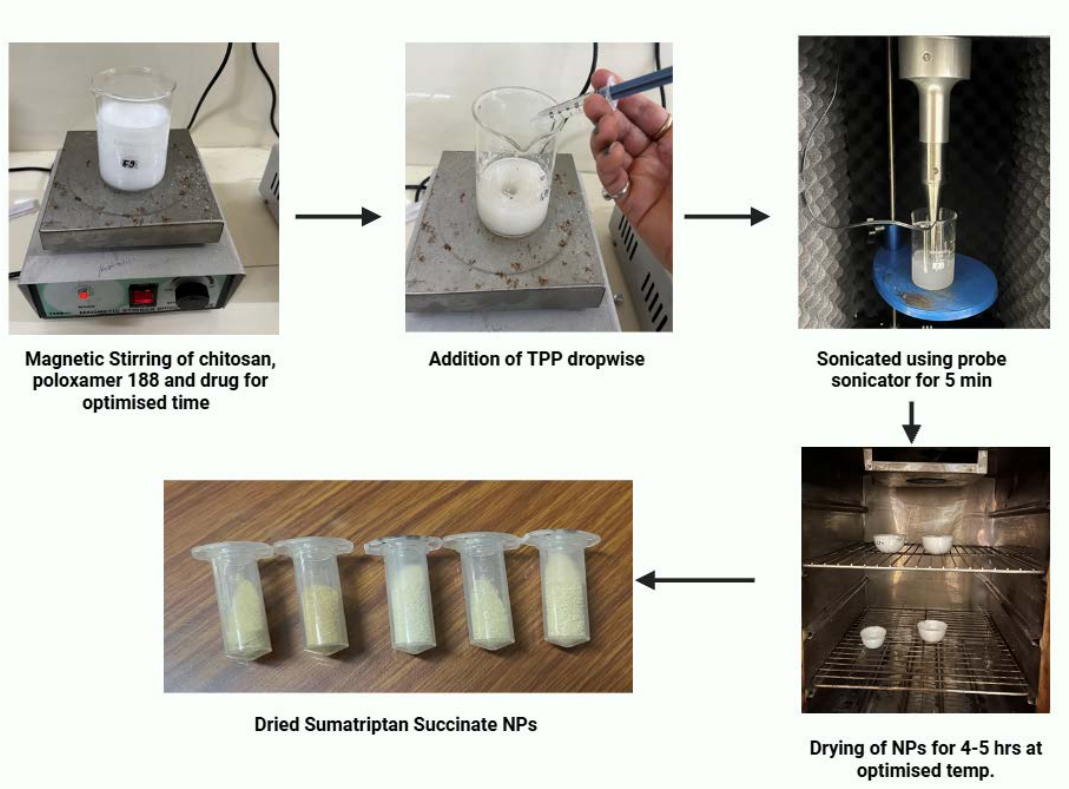

Figure 1: Diagrammatic representation of the ionic gelation method for NPs preparation

CHARACTERIZATION OF SS-NPS

Entrapment Efficiency EE % and Drug Loading DL%

To determine the drug content in the nanoparticles, a 10 mL dispersion of the nanoparticles was centrifuged. The unbound drug molecules were separated from those contained within the nanoparticle dispersion by centrifugation (20 minutes at 4500 rpm). To measure the amount of free drug in combination, a UV spectrophotometer was used to analyze the separated and diluted supernatant. The measured amount was then subtracted from the total amount of medication that was initially added. The EE percentage was computed as;

$$EE = \frac{(W\ (initial\ drug)\ - W\ (free\ drug)}{W\ (initial\ drug)} \times 100$$

0.3 ml sample of the NPs formulation was initially diluted to determine the drug loading. The same solvent was used to create more dilutions. A UV-visible spectrophotometer set to 227 nm was then used to measure the drug content in these diluted samples. For this aim, specific formulas were used to calculate the percentages of DL [23].

$$DL\ (\%) = \frac{Amount\ of\ drug\ encapsulated\ in\ nanoparticles}{Total\ weight\ of\ nanoparticles} \times 100$$

Particle Size, PDI, and Zeta potential

Using photon correlation spectroscopy (PCS) and a Zetasizer Nano ZS-90 (Malvern Instruments, Worcestershire, UK), the particle size distribution and Zeta potential were ascertained. The degree of uniformity in particle-size distribution within the formulation was evaluated using the PDI. The surface charge properties of the nanoparticles, which are crucial factors in determining colloidal stability and their interaction with biological membranes, were revealed by zeta potential analysis [24].

Transmission electron microscope (TEM)

The size, shape, and morphology of the prepared NPs were examined using TEM. A carbon-coated copper grid was filled dropwise with the NP suspension. The NPs were then examined using electron diffraction and a TEM operating in bright-field mode at a voltage of 200 kV [23].

Method of preparation of SS-NPs loaded *in situ* gel

The cold procedure was used to create the gel. To completely dissolve Poloxamer 407 (18–22% w/v), it was dissolved in cold distilled water in a glass beaker and kept at 4 °C. After being dissolved in water for a whole day, carbopol 934P (0.2–0.5% w/v) was added to the poloxamer solution while being continuously stirred[25]. SS-NPs, a solubilizer (13–15% w/v), and the preservative methylparaben (0.05%) were added to the prepared gelling solution to improve it. As seen in Figure 2, the formulation was constantly agitated with a magnetic stirrer to create a homogenous solution [26]. All formulation steps were performed under refrigerated conditions (4–8 °C) to prevent premature thermoactivation of Poloxamer 407.

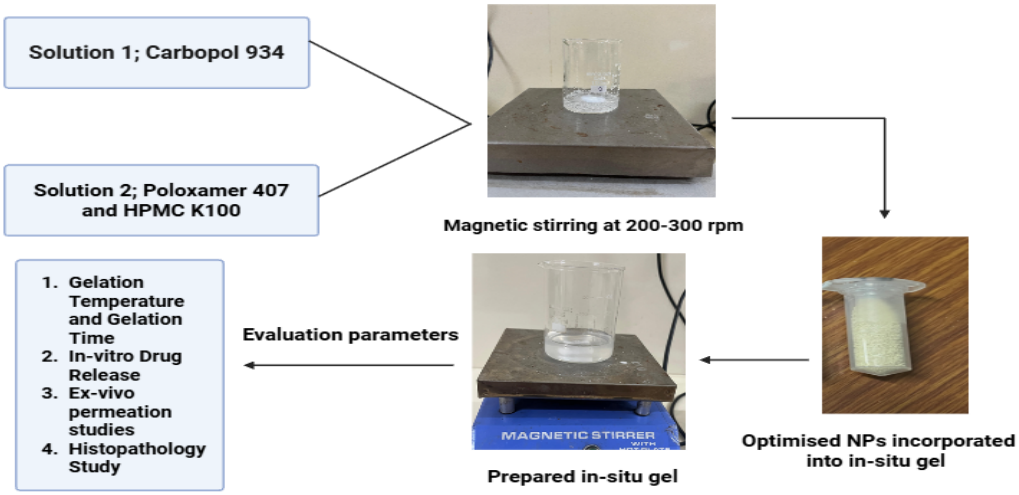

Figure 2: Preparation of sumatriptan succinate Cs-NPs loaded *in situ* gel

CHARACTERIZATION OF SUMATRIPTAN NANOPARTICLE-LOADED *IN-SITU* GEL (SS-NPG)

Physicochemical properties of gel

Immediately following formulation, the pH of the optimized *in situ* nasal gel was measured using a calibrated digital pH meter (Digital pH Meter 335, Techno Scientific Products, Bangalore, India). To evaluate the formulation's appearance and clarity under suitable lighting, a visual examination was conducted. To detect suspended particles, fibers, or indications of turbidity, the sample was gently inverted against contrasting black and white backgrounds to investigate swirling behavior [27]. The gel was rheologically evaluated at 30 ± 1 °C with a spindle speed of 20 rpm using a Brookfield viscometer (LVDV-I Prime, Middleborough, MA, USA).

Drug content

After precisely weighing and transferring the nanoparticle-loaded *in situ* gel (1 g) into a 15 mL centrifuge tube, methanol was added to extract the drug from the polymeric matrix. Until the mixture was completely soluble, it was vortex-mixed. To

eliminate undissolved excipients, the resultant solution was centrifuged after being suitably diluted with methanol. A UV-visible spectrophotometer was used to measure the filtrate's absorbance at the specified wavelength after the supernatant was filtered through a membrane filter [28]. A previously created calibration curve was used to calculate the drug content.

Gelation temperature

A visual technique was used to determine the sol–gel transition temperature of the formulations. In short, a glass vial with a magnetic stir bar was filled with 5 mL of each mixture and sealed. The temperature was progressively increased from 20 °C to 40 °C while the vials were submerged in a thermostatically regulated water bath. A calibrated thermometer with a sensitivity of 0.1 °C was used to measure the temperature. A constant stirring speed of about 80 rpm was maintained. The temperature at which the magnetic stir bar stopped rotating, signifying the change from the sol to the gel state, was known as the gelation temp. [29].

Entrapment Efficiency

Take a precisely calculated amount of drug-loaded nanoparticle-containing *in situ* gel (such as 1 g or 1 mL). To dissolve the gel and release the nanoparticles into suspension, add an appropriate volume of buffer or solvent (usually phosphate buffer, pH 6.4–7.4). If necessary, sonicate until the gel base is completely dissolved. To sediment the nanoparticles, centrifuge the suspension at a high speed (e.g., 15,000 rpm for 30–45 min at 4°C). The medication is free (unentrapped) in the supernatant. Gather the supernatant and use a UV-Vis spectrophotometer to measure absorbance at the drug's λ max [30].

Thermal Analysis (DSC)

A DSC-60 device (Shimadzu Corporation, Kyoto, Japan) was used to examine the sample's thermal behavior. In an inert atmosphere, precisely weighed samples (about 10 mg) were sealed in standard aluminum pans and analyzed over the temperature range of 50–300 °C at a controlled heating rate of 10 °C/min. The obtained thermograms were analyzed to find distinctive thermal transitions and evaluate any possible alterations in thermal stability or crystallinity [30].

***In vitro* drug release**

A Franz diffusion cell with an effective diffusion area of 1.3 cm^2 was used to assess in vitro drug release. The receptor medium was simulated nasal fluid (pH 6.8), and a cellophane dialysis membrane (MWCO 12–14 kDa) was placed between the donor and receptor compartments and soaked beforehand. The donor compartment was filled with the prepared *in situ* gel (5 mL). Twenty milliliters of simulated nasal fluid were added to the receptor chamber, which was kept at 37 ± 0.5 °C with constant stirring at 50 rpm. To maintain sink conditions, aliquots were removed at prearranged intervals over eight hours and promptly replaced with an equivalent volume of fresh medium. After appropriate dilution, the samples obtained were subjected to spectrophotometric analysis at the specified wavelength. The best-fit model was chosen based on the correlation coefficient (r^2) and release exponent values after drug release data were fitted to a variety of kinetic models, such as zero-order, Higuchi, and Korsmeyer–Peppas models [31].

Kinetic release data

A dissolution data (DD) solver was used to study the drug-release kinetics of the optimized formulations. To determine the most suitable mechanism governing drug release based on the best statistical fit, the release profiles were fitted to a variety of kinetic models, including zero-order, first-order, Higuchi, Korsmeyer–Peppas, and Hixson–Crowell models.

Similarity Factor (f_2)

The conditions for the SS tablets' in vitro drug-release profile were comparable to those for the SS-NPs ISG4 test formulation. The similarity factor between the two formulations was evaluated using the medication release profile data. The similarity factor was evaluated using the DD solver software 26.

***Ex vivo* permeation studies**

Freshly removed goat nasal mucosa from a nearby abattoir was used for ex vivo permeation investigations. The superior nasal concha was carefully isolated after the nasal septum was removed. Before the experiment, the removed mucosa was allowed to settle in simulated nasal fluid (SNF, pH 6.8) for one hour. After that, the hydrated mucosal tissue was positioned with its epithelial surface facing the donor compartment between the donor and receptor compartments of a Franz diffusion cell. Both containers were first filled with SNF and agitated for 15 minutes using a magnetic stirrer to stabilize the tissue. After that, a new SNF (25 ml) was added to the receptor compartment in place of the medium. The donor compartment was filled with a set volume (0.5 ml) of formulation. The receptor medium was

continuously stirred and maintained at 37 ± 0.5 °C. Samples were collected at prearranged intervals and, after appropriate dilution, analyzed spectrophotometrically at 227 nm [31].

Cell Culture

The National Centre for Cell Science (NCCS) in Pune, India, provided the human nasal epithelial cell line RPMI-2650, which was generated from nasal septum squamous cell carcinoma. Minimum essential medium (MEM) containing 10% (v/v) fetal bovine serum (FBS), 1% (v/v) antibiotic–antimycotic solution, and non-essential amino acids was used to cultivate the cells. Cultures were kept in a humidified incubator with 5% CO2 at 37 °C. The study used passages up to P28 and subcultured cells every 48 hours. Cells were separated using a trypsin–EDTA solution (0.025% trypsin, 0.01% EDTA in DPBS) once they reached about 80% confluence. A hemocytometer was used to measure cell number and viability, and T-25 flasks were seeded at the required cell density for subsequent in vitro tests. [32,33].

Cell viability and proliferation studies: MTT assay

RPMI-2650 human nasal epithelial cells were used in the MTT assay to evaluate the cytotoxic potential of the produced formulations. To facilitate cell adhesion, cells were seeded in 96-well plates at a density of 1.5×10^2 cells/well in 200 µL of complete medium and incubated at 37 °C overnight. After that, a new MEM with different concentrations of the test formulations was used in place of the culture medium. The positive control was Triton X-100 (0.1% v/v), and the negative control was untreated cells. Following a 24-hour incubation period under standard culture conditions (37 °C, 5% CO_2), the treatment media were removed, and the cells were incubated for 3 hours with 100 µL of MTT solution (0.5 mg/ml). A microplate reader (ELx800, BioTek, USA) was used to measure absorbance at 570 nm after dissolving the formazan crystals in 100 µL of DMSO. In comparison to untreated control cells, cell viability was expressed as a percentage [34]. Cell viability percentage is determined using the following formula:

$$\%\ \boldsymbol{cell\ viability} = \frac{\boldsymbol{OD\ of\ treated\ cells}}{\textbf{OD of Untreated cells}} \times \mathbf{100}$$

The linear regression equation, Y = Mx + C, was used to calculate the IC50 value. In this case, the viability graph was used to determine Y = 50, M, and C values.

Cell morphological assessment

To evaluate cellular compatibility, morphological alterations in RPMI-2650 cells after exposure to the test formulations were investigated. The formulation was applied to cells at different concentrations (31.25–500 µg/ml), and they were incubated at 37 °C for 24 hours. An inverted biological microscope (CKX-41, Olympus, Tokyo, Japan) with a digital imaging system was used to examine cellular morphology following treatment. MICAM software was used to capture images at 20× magnification to document any changes in cell morphology, integrity, or attachment. 100 µm was represented by the scale bar [35,36].

Histopathology Study

The nasal mucosa of a freshly removed goat was divided into four equal segments, and each segment was incubated for two hours with the nanoparticle-loaded formulation (3 ml), plain drug solution (3 ml), simulated nasal fluid (3 ml; negative control), and isopropyl alcohol (3 ml; positive control). To remove any remaining formulation, the tissues were carefully cleaned three times with distilled water after incubation. Following processing, the samples were sectioned and stained with hematoxylin & eosin. An optical microscope (Olympus BX51, Tokyo, Japan) was used to analyze histological slides made by a certified pathologist to evaluate any morphological changes or epithelial damage to the nasal mucosa [37,38].

Stability Studies

In compliance with International Council for Harmonization of Technical Requirements (ICH) recommendations, short-term stability tests were conducted on the optimized formulation. For two months, the formulation was kept at 25 ± 2 °C and 40 ± 5% relative humidity. Samples were taken out at prearranged intervals and assessed for EE, PDI, and particle size to establish the formulation's physicochemical stability during storage [37].

RESULT AND DISCUSSION

Solubility Profile

The prepared solution was exposed to UV light to determine its absorbance at 227 nm. According to the standard table provided in I.P. (2022), the observed solubility data were compared and documented in Table 2.

Table 2: Solubility profile of SS in different solvents

SN	Solvents	Conc.	Solubility
1	Water	20 mg/ml	Freely Soluble
2	Phosphate buffer 6.8	10 mg/ml	Freely Soluble

All solvents derived from the test sample yield solubility data within the specified range, thereby confirming the substance's purity.

Optimization

Using BBD design-experiment software, optimized Sumatriptan succinate NPs. Seventeen experiments were generated and conducted with Design-Expert13 software, including different quantities of (A) Chitosan, (B) Poloxamer 188, and (C) sodium tripolyphosphate (STPP) as shown in Table 3. All formulations have been developed and evaluated for dependent responses, namely EE(R1), DL(R2), and DR(R3), as seen in Table 3. The response values from all runs were analyzed using linear, second-order, and quadratic models, with the quadratic model providing the best fit for each response ($p < 0.0001$). A regression study for each model, considering both responses, was conducted, with the results presented in Table 4. An ANOVA was conducted to determine the optimal fit for both responses. ANOVA identifies the significant ($p < 0.05$) and insignificant ($p > 0.05$) impacts of each variable on the responses (EE, DL, and DR). Response surface graphs were generated for each response, illustrating the influence of several parameters on the response Figure 3.

Table 3: BBD matrix and observed responses of Cs- NPs

Formulation	A: Chitosan (mg)	B: Poloxamer 188 (mg)	C: STTP (mg)	R1: EE (%)	R2: DL (%)	R3: DR (%)
NP1	0.55	1	1.05	74.33	12.32	73.67
NP2	0.1	1	2	79.45	14.65	88.56
NP3	0.55	0.5	0.1	84.41	11.22	68.21
NP4	0.55	0.5	2	85.03	11.41	80.43
NP5	0.1	1.5	1.05	72.45	14.21	74.98
NP6	1	0.5	1.05	74.55	10.24	72.56
NP7	0.55	1.5	0.1	84.44	11.19	69.56
NP8	0.1	1	0.1	83.21	13.67	71.89
NP9	0.1	0.5	1.05	72.31	13.76	72.39
NP10	0.55	1	1.05	72.11	11.44	71.65
NP11	0.55	1	1.05	73.61	12.19	74.67
NP12	0.55	1	1.05	75.11	12.12	76.78
NP13	0.55	0.5	1	89.09	14.33	90.26
NP14	1	1.5	1.05	74.21	10.31	76.92
NP15	0.55	1	1.05	75.43	12.21	85.89
NP16	1	1	0.1	82.28	10.45	72.56
NP17	0.55	1.5	2	84.33	12.29	83.78

Table 4: Summary of Regression Analysis Findings for Variables R1, R2, and R3

	EE%	DL%	DR%
Std. Dev.	1.03	0.271	1.94
R2	0.9832	0.9829	0.9799
Adjusted R2	0.9915	0.9909	0.9940
Predicted R2	0.9820	0.9835	0.9885
Mean	78.37	12.02	78.02
C.V.%	1.31	2.26	2.49
Adeq. Precision	66.36	31.45	38.60

Diagnostics: Residual vs Run

Figure 4 shows diagnostic plots to evaluate the sufficiency, predictive capability, and reliability of the developed quadratic models for EE, DL, and DR. The projected-versus-real graphs (top panels) show a strong correlation between experimental values and model predictions for all three reactions. In both cases, the data points are closely aligned with the 45° reference line, indicating minimal prediction error and strong predictive ability. The high coefficients of determination (R2) also support the accuracy and consistency of the developed models for EE, DL, and DR.

The residual vs run plots (bottom plots) were examined to assess the randomness of the residual distribution and the possible presence of systematic patterns or deficiencies in the model. For EE and DL, the residuals were randomly distributed around the zero line, and most were within the control limits, indicating that the models effectively explained the variability in the experiment. One major deviation was observed in an experiment involving EE and DL, which could be due to slight experimental variability, such as formulation differences, instrument sensitivity, or minor procedural errors. However, these individual anomalies did not indicate any systemic prejudice or the overall lack of integrity of the models. The case of DR showed no outliers or discernible patterns, and the residuals were identically and randomly distributed across all experiment runs; therefore, the exceptional model stability and predictive reliability of this response are affirmed. The comparison between the projected and actual plots, along with residual diagnostics, demonstrates that the developed models are statistically sound, exhibit no significant lack of fit, and can reliably predict and optimize EE, DL, and DR.

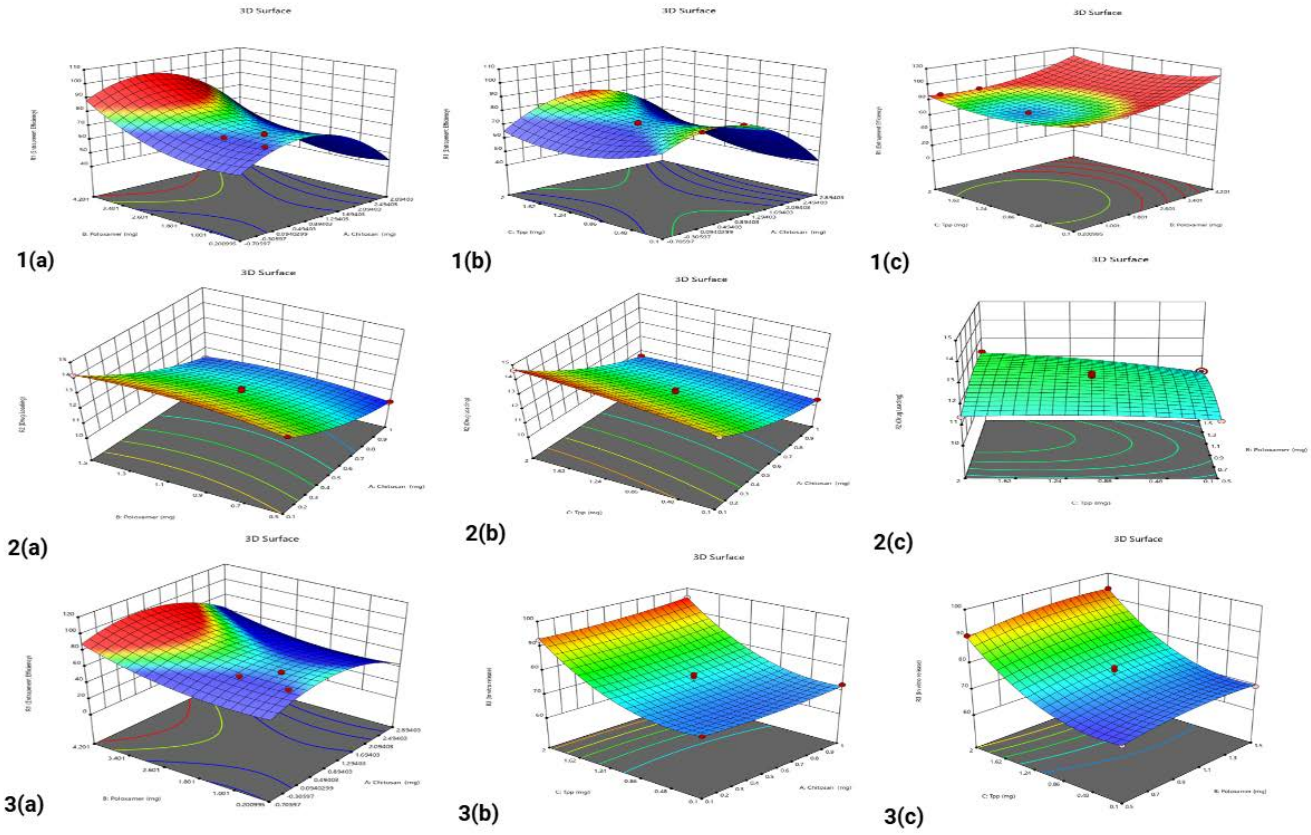

Figure 3: Representation of response surface graph (1) Entrapment efficacy, (2) Drug loading, and (3) Drug release, with respects to independent variables chitosan (A), poloxamer (B), and STPP (C)

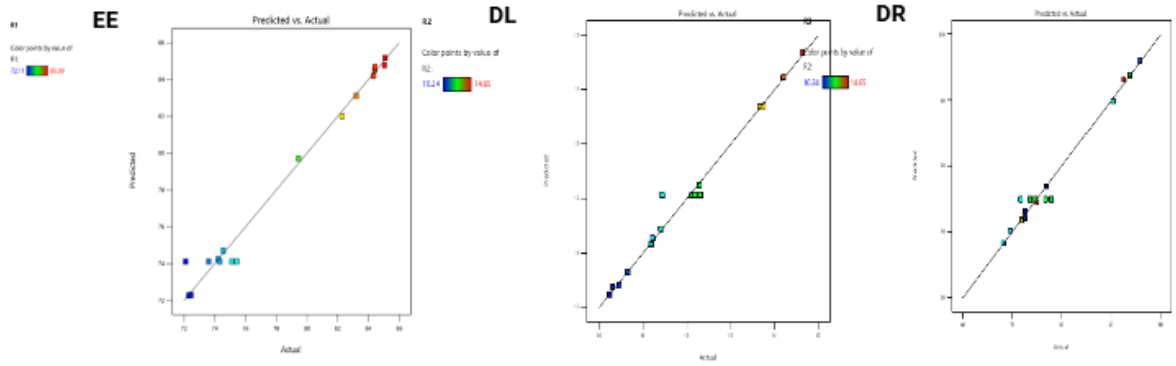

Figure 4: Graphical Representation of Residuals Across Experimental Runs to Evaluate Model Stability & Accuracy

Effect of chitosan, poloxamer, and STPP on the EE of NPs

The resulting equation illustrates the influence of each factor level on EE-

$$Y= 74.12+ 1.09A- 0.1088B- 0.0550C- 0.1200AB +1.63AC- 0.1825BC- 1.39A^2+ 0.6535B^2+ 9.78C^2$$

The regression model has shown that B, C, AB, B^2, and BC were non-significant ($p > 0.05$), but the other values had a significant influence on the nanoparticle's EE%. The quadratic model had the best fit ($F = 45.42$, $p < 0.0001$) the lack of fit was insignificant ($F = 0.0676$, $p > 0.05$). The very close adjusted R^2 (0.9915) to the predicted R^2 (0.9820), along with the low CV (1.31) and high acceptable accuracy (66.36), demonstrated the model's sustainability, as shown in Table 4. EE% formulation range was between 72.11 and 89.09%. The linear terms show that chitosan (A) increases EE, probably due to matrix formation

and drug encapsulation. Poloxamer (B) and STPP (C) exhibit significant negative effects, suggesting that increasing their concentrations could reduce EE by disrupting nanoparticle crosslinking or causing drug leakage. Chitosan and STPP (AC) interact positively, suggesting that their combined usage increases retention owing to efficient ionic crosslinking between their amine and phosphate groups. Chitosan, poloxamer (AB), and poloxamer and STPP (BC) had negative effects, suggesting they could reduce EE by interfering with particle formation. Chitosan (A^2) has a negative value, suggesting that higher concentrations may reduce EE owing to viscosity or particle aggregation. However, poloxamer (B^2) and STPP (C^2) exhibit positive quadratic effects, indicating improved EE via crosslinking and enhanced particle stability at higher doses.

Effect of chitosan, poloxamer, and STPP on the DL of NPs

The resulting equation illustrates the influence of each factor level on DL-

$$Y= 12.06- 1.83A- 0.1713B+ 0.3100C- 0.0950AB - 0.1925AC+0.2275BC+0.4520A^2- 0.3780B^2-0.1505C^2$$

Regression analysis showed that B, AB, AC, BC, and C2 were non-significant (p=.05), whereas the other parameters had a significant effect on drug loading (DL). The quadratic model had the best fit ($F = 44.72$, $p < 0.0001$) with an insignificant lack of fit ($F = 0.0549$, $p > 0.05$). The model's good forecasting ability was confirmed by the adjusted R2 (0.9909) being close to the expected R2 (0.9835), the low coefficient of variation (2.26%), and a high acceptable precision (31.45), as shown in Table 4. Formulations with varying amounts of DL ranged from 10.24% to 14.65%. Chitosan shows the greatest negative effect among linear variables, indicating that increasing chitosan concentration significantly lowers DL. Increased matrix density or viscosity may impact drug encapsulation. Poloxamer suggests DL may decrease at high dosages owing to drug-polymer interactions.

STPP has a moderate beneficial effect, likely due to improved crosslinking, which stabilizes particles and increases drug retention. Increases in chitosan–poloxamer and chitosan STPP reduce DL due to unfavorable interactions. Denser particle arrangements may reduce the area available for drug trapping. The positive interaction between poloxamer and STPP suggests a synergistic effect that may boost DL by stabilizing drug incorporation or particle formation. The quadratic terms show that chitosan has a positive quadratic effect, but at an optimal concentration, it may reduce DL due to increased polymer entrapment. Poloxamer and STPP had negative quadratic effects, suggesting that particle instability or drug ejection reduces drug loading efficiency at higher doses.

Effect of chitosan, poloxamer, and STPP on the DR of NPs

The resulting equation illustrates the influence of each factor level on DR-

$$Y= 74.93+0.7638A+ 1.46B+ 11.31C+ 0.4425AB +0.6650AC+0.5000BC+1.01A^2- 1.72B^2+7.29C^2$$

Regression analysis showed that the non-significant variables included A, B, AB, AC, BC, A2, and B2 ($p > 0.05$), whereas other parameters significantly influenced drug release (DR) across the considered models. The quadratic model showed the best fit ($F = 37.86$, $p < 0.0001$) with insignificant lack of fit ($F = 0.0988$, $p > 0.05$). The high concordance between the adjusted R2 (0.9940) and the projected R2 (0.9885), along with a low coefficient of variation (2.49) and a high level of acceptable precision (38.60), confirms the model's strength and reliability, as shown in Table 4. The drug release from the formulations ranged from 71.65% to 85.26%.

The linear variable STPP has the greatest positive effect, indicating that drug release improves significantly with STPP concentration. More porous or hydrophilic networks may increase drug diffusion. Poloxamer has a positive effect, suggesting that higher dosages increase drug release via dissolving and swelling the system. Chitosan has a small but positive effect, showing that matrix integrity affects drug release. Chitosan and poloxamer, Chitosan and STPP, and poloxamer STPP show positive coefficients, suggesting that these variables synergistically increase drug release. This shows that modifying these variable pairs simultaneously could enhance drug release, possibly due to balanced gel and perfect particle size. However, poloxamer shows a negative quadratic effect, suggesting that excessive gelation or drug diffusion route modification could affect drug release.

Selection of the Optimized Batch

The optimized drug-loaded nanoparticle formulation was prepared by using BBD in conjunction with a desirability function approach to maximize EE, DL, and DR. The model predicted optimal responses of 92.32% EE, 14.65% DL, and

92.88% DR, corresponding to a desirability value of 0.001. To validate the predictive model, three independent batches were prepared under the optimized formulation parameters. The experimental outcomes, yielding 89.09% EE, 14.33% DL, and 90.26% DR, demonstrated close concordance with the predicted values, thereby confirming the robustness of the optimization strategy. The residuals between predicted and observed results were 3.49 for EE, 0.073 for DL, and 2.62 for DR. The bias percentages were calculated using the formula:

$$\textbf{\textit{Bias}}\ (\%) = \frac{[(\textbf{\textit{Predicted value}} - \textbf{\textit{Observed value}}) \times \mathbf{100}]}{\textbf{\textit{Observed value}}}$$

yielding values of 3.9% for EE, 2.2% for DL, and 2.90% for DR are mentioned in Table 5.

Table 5: Constraints and goals aimed at the dependent variables

Dependent variables	Constraints	Goal	Obtained value	Predicted value	Residuals	Bias (%)
EE	72.11 to 89.09	Maximum	89.09%	92.32%	3.49	3.9%
DL	10.24 to 14.65	Maximum	14.33%	14.65%	0.073	2.2%
DR	68.21 to 95.89	Maximum	90.26%	92.88%	2.62	2.90%

EVALUATIONS OF OPTIMISED NANOPARTICLES

Entrapment Efficiency and Drug Loading (%)

The EE of the chitosan nanoparticles was found to range from 72.11% to 89.09%, respectively, indicating effective incorporation of sumatriptan succinate within the polymeric matrix. The extent of drug entrapment is strongly influenced by the physicochemical properties of both the polymer and the drug, as well as their intermolecular interactions. Chitosan, owing to its hydrophilic nature, facilitates favorable interactions with the water-soluble sumatriptan succinate, primarily through hydrogen bonding between the amino groups of chitosan and functional groups of the drug. Furthermore, the ionic crosslinking process between negatively charged tripolyphosphate and positively charged chitosan and drug molecules significantly enhances drug loading. This electrostatic interaction promotes efficient drug retention within the nanoparticulate network, thereby improving encapsulation efficiency and supporting the suitability of chitosan nanoparticles for nasal delivery of hydrophilic antimigraine agents. The optimized formulation has a drug loading of 10.24% to 14.65%, which is enough for intranasal administration of Sumatriptan. The usual therapeutic dose of Sumatriptan given through the nose is 10 to 20 mg per dose, and the most that can be placed in each nostril is about 0.1 to 0.25 mL (about 0.2 to 0.5 mL total). Because Sumatriptan is quite potent and the mucoadhesive nanoparticle-loaded in situ gel facilitates drug entry and retention in the nasal cavity, a drug loading of 14.33% is sufficient to deliver the drug into this small space. Nanoparticle-based administration also helps keep the drug in the body longer and makes it easier for it to travel from the nose to the brain. This could mean that the systemic dose needed is lower than with traditional formulations. Although the nasal cavity is small, the amount of drug loaded is clinically significant and can effectively treat migraines intranasally.

Particle size, PDI, and Zeta potential

The optimized nanoparticle formulation had a mean particle size of 154.3 nm and a PDI of 0.3485, indicating that the particles weren't highly polydisperse. Most systems with PDI values below 0.3 are quite similar. The PDI values are usually slightly higher when polymeric nanoparticles are prepared via ionic gelation, particularly with chitosan. This is because, at higher polymer concentration, viscosity and coacervate formation are also higher. There was a clear peak in the size distribution profile, and no aggregation. This means that the particles were produced in a controlled manner and that the batch was quite precise. Nanoparticles smaller than 200 nm are effective for nasal entry. The potential physical stability of nanoparticle dispersion is closely associated with the zeta potential. ZP represents the total charge accumulated by the particles. A greater reached value correlates with increased system stability. The value of ± 30 mV enhances system stability, since all particles will reject one another due to the significant negative or positive zeta potential in the dispersion medium. The formulated preparation exhibited a ZP value of +22.79 mV, indicating the generation of nanoparticles with commendable physical and chemical stability, as shown in Figure 5.

TEM

TEM analysis revealed the morphological characteristics and particle size distribution of the prepared chitosan-poloxamer nanoparticles. Figure 6 shows well-defined, spherical nanoparticles with sizes ranging from approximately 28.5 nm to 290 nm. The presence of both smaller (28.5–74.2 nm) and

relatively larger particles (~290 nm) suggests a polydisperse system, which may result from aggregation or partial swelling of the polymer matrix. The spherical morphology and nanoscale dimensions are favorable for intranasal delivery, facilitating enhanced mucosal penetration and potential transport to the brain via the olfactory pathway. The structural integrity and uniform appearance of the particles indicate successful formulation and suitability for nasal drug delivery applications

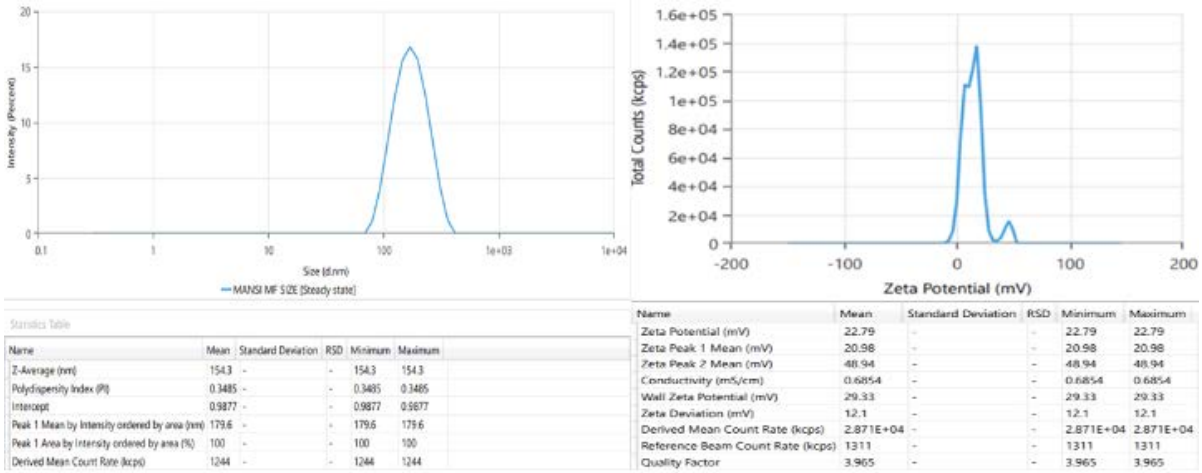

Name	Mean	Standard Deviation	RSD	Minimum	Maximum
Z-Average (nm)	154.3	-	-	154.3	154.3
Polydispersity Index (PI)	0.3485	-	-	0.3485	0.3485
Intercept	0.9877	-	-	0.9877	0.9877
Peak 1 Mean by Intensity ordered by area (nm)	179.6	-	-	179.6	179.6
Peak 1 Area by Intensity ordered by area (%)	100	-	-	100	100
Derived Mean Count Rate (kcps)	1244	-	-	1244	1244

Name	Mean	Standard Deviation	RSD	Minimum	Maximum
Zeta Potential (mV)	22.79	-	-	22.79	22.79
Zeta Peak 1 Mean (mV)	20.98	-	-	20.98	20.98
Zeta Peak 2 Mean (mV)	48.94	-	-	48.94	48.94
Conductivity (mS/cm)	0.6854	-	-	0.6854	0.6854
Wall Zeta Potential (mV)	29.33	-	-	29.33	29.33
Zeta Deviation (mV)	12.1	-	-	12.1	12.1
Derived Mean Count Rate (kcps)	2.871E+04	-	-	2.871E+04	2.871E+04
Reference Beam Count Rate (kcps)	1311	-	-	1311	1311
Quality Factor	3.965	-	-	3.965	3.965

Figure 5: Particle size, PDI, and Zeta potential of optimized SS-NPs

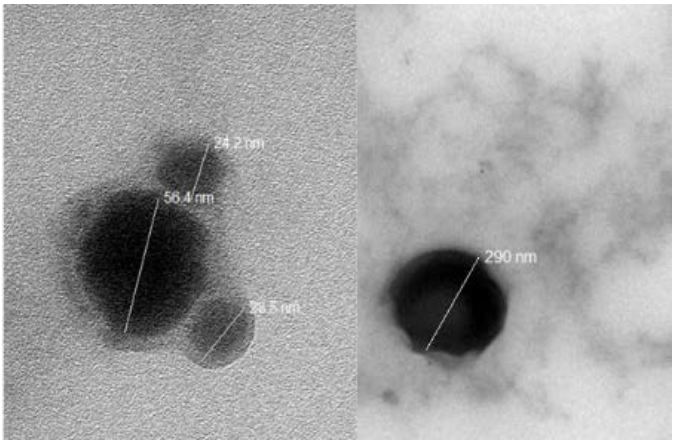

Figure 6: TEM images of optimized SS-NPs

Development of SS-NP *In Situ Gel*

The SS-NP13 *in situ* gel was formulated with varying amounts of the thermos-responsive polymer, poloxamer 407, and varying concentrations of carbopol 934P.

EVALUATIONS OF SS-NP *IN SITU GEL*

Physicochemical properties of gel (pH and Viscosity)

The pH of all formulations was determined to be in the range of 5.8 ± 0.3 to 6.8±0.5, which is within the nasal pH range of 6.2±0.21 to 6.8±0.44 Table 6. This ensures that all formulations were compatible with the nasal mucosa. All formulations were clear, indicating that clarity is inversely related to the concentration of carbopol 934 incorporated in the formulations. The sol viscosity of all the formulations ranged between 48-84 cp, respectively, while the gel viscosity was measured to be 217±15 to 589±22 cp at 37 °C Table 6. Increasing polymer concentration strengthens the gel matrix, increases viscosity, enhances muco-adhesion, and controls drug release. The combined action of thermos-responsive gelling (Poloxamer) and ionic crosslinking (Chitosan-STPP) results in optimal viscosity for nasal delivery.

Gelling temperature, EE (%) and DC (%)

Thermo-reversible gels are an established drug-delivery technique for nasal administration, as they retain the drug within the cavity for an extended period without facilitating its release from the dosage form. If the gelling temperature exceeds nasal temperature, the formulation may be expelled from the nose; conversely, if it is below 21-22°C, it may pose difficulties in handling and transportation. Table 6 depicts the gelling temperature of all synthesized SS-NP *in situ* gels. It was noticed that an increasing polymer concentration results in a decreasing gelling temperature. The results indicate that a 18% concentration of poloxamer 407 is optimal for in situ gel formation, with gelation at 28–34 °C. The Poloxamer 407 solution undergoes a phase shift, resulting in gel formation at temperatures below 34°C. Poloxamer 407 exhibits phase separation properties due to its negative solubility coefficient in block copolymers. The rise in temp. is directly proportional to the development of micelles, resulting in the construction of densely packed micelles that later form a gel. The EE ranged

from 78±0.33 to 85±0.42%, as shown in Table 6, indicating excellent drug encapsulation within the SS-NP in situ gel and thereby validating the system's potential for controlled nasal administration. The drug concentration of the formulated *in situ* gels was quantified using a UV-vis spectrophotometer (UV 1800, Shimadzu, Japan) at 227 nm, yielding values ranging from 88.12±0.33% to 95.82±0.66%, as shown in Table 6.

Table 6: Results of SS NP *In Situ* Gel Formulations

Batch	Conc. of Poloxamer 407(%)	Conc. of Carbopol (%)	pH	Viscosity (cps)		EE (%)	DC (%)	Gelation Temp (°C)
				At 25°C	At 34°C			
SS-NP13IG1	12	0.1	6.5±0.28	48±0.27	217±0.32	78±0.33	88.12±0.33	No Gelation
SS-NP13IG2	14	0.2	6.2±0.21	55±0.55	345±0.29	75±0.82	91.73±0.48	No Gelation up to 40 °C
SS-NP13IG3	16	0.3	6.4±0.13	59±0.71	444±0.45	81±0.51	93.20±0.54	Gelation at 30 °C
SS-NP13IG4	18	0.4	6.8±0.44	62±0.92	556±0.42	85±0.42	95.82±0.66	Gelation at 28-34 °C
SS-NP13IG5	20	0.5	6.2±0.29	57±0.33	589±0.17	83±0.29	92.22±0.71	Gelation at 25-31°C

DSC

DSC is an essential tool for measuring the physical state of a drug within a carrier system. The presence of a sharp, well-defined melting endotherm in the thermogram of the pure drug confirms its crystalline nature. On the other hand, if this peak disappears, widens, or shrinks significantly in the nanoparticle formulation, it could indicate that the drug is becoming amorphous or spreading out in the carrier matrix, as shown in Figure 7. It is important to know whether the drug is in a crystalline or amorphous form, as this affects how well it dissolves, how stable it is, and how available it is to the body. An amorphous or molecularly dispersed form often improves dissolution and drug release. This is especially significant for delivery systems that target the brain or are administered intranasally. A comparative thermogram measurement thus offers scientific validation of effective drug integration and supports predictions regarding enhanced formulation effectiveness.

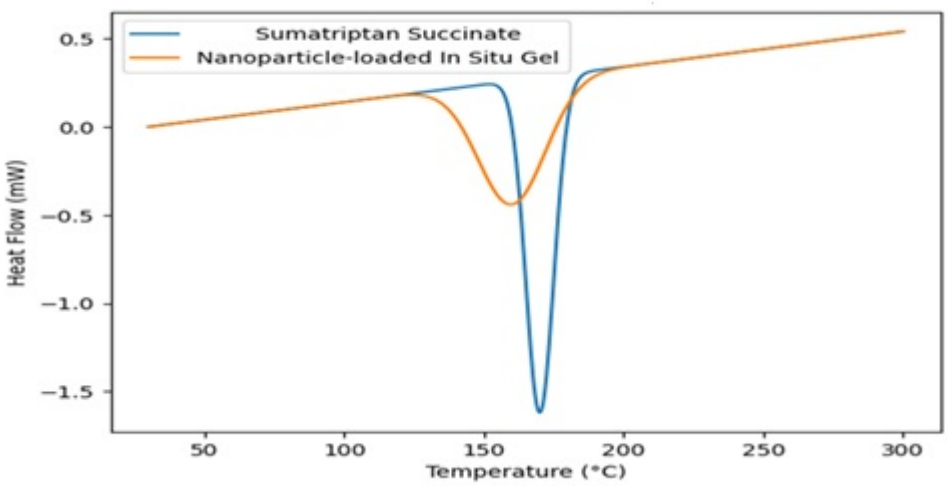

Figure 7: DSC comparison of SS and SS-NPs *In-situ* gel

***In vitro* drug release studies**

The *in vitro* release of Nanoparticles (SS-NP13) and *in situ* gel (SS-NP13G4) was conducted using a dialysis bag. The optimized SS-NP13 release exhibits a rapid release rate of 90.26 ± 0.76% within 10 hrs. The SS-NP13G4 exhibited a dual release profile, characterized by an initial burst release of 30.54 ± 0.87%, which is beneficial for delivering the loading dose necessary to attain the desired therapeutic concentration, followed by a sustained release of 88.89 ± 0.98% over 10 hours, which can help maintain therapeutic concentration over an extended duration, as shown in Figure 8.

The incorporation of nanoparticles into gels may be the cause of the drug's delayed release in the case of SS-NPG4. The findings indicated that adding polymeric nanoparticles to the gel creates an additional barrier to drug transport. Furthermore, the sustained-release mechanism indicated that the drug was encapsulated within the polymeric NPs.

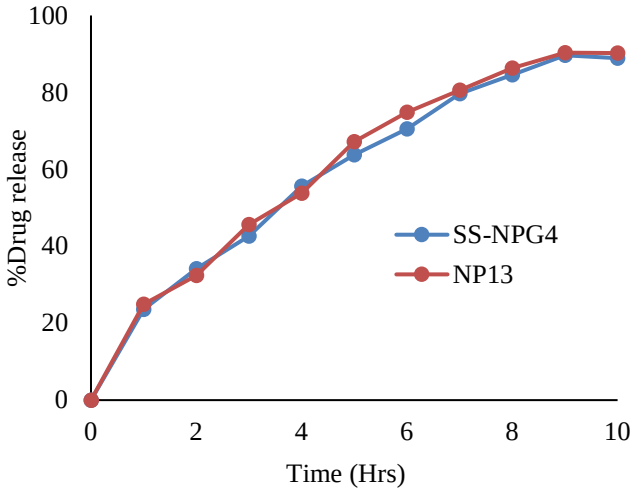

Figure 8: *In vitro* drug release of Optimized SS-NPG4 and Optimized NP13

Kinetic Analysis

The in vitro release kinetics of optimized formulation (SS-NP13IG4) were analyzed using DD Solver as shown in Figure 9. The release data were fitted to multiple kinetic models, including zero-order, first-order, Higuchi, and Korsmeyer–Peppas, and the corresponding correlation coefficients (R^2), adjusted R^2, sum of squared residuals (SSR), and model selection criterion (MSC) values were calculated in Table 7. Among the evaluated models, the Korsmeyer–Peppas model provided the best fit, as evidenced by the lowest SSR (41.3131), the highest R^2 (0.9953), and the highest adjusted R^2 (0.9948). Furthermore, the model exhibited the highest MSC value (4.5284), confirming its superior descriptive capability. If n < 0.85, the transport is non-Fickian (anomalous). In our experiment, the release exponent 'n' is 0.610, suggesting that drug release is governed by both diffusion and polymer relaxation/erosion, rather than by diffusion alone or by swelling.

Table 7: Kinetic Release Data

Release Model	R^2	R^2 adjusted SSR	MSC
Zero-order	0.8804	0.8804	1.4682
First order	0.9898	0.9898	3.9269
Higuchi	0.9820	0.9820	3.3592
Korsmeyer-peppas	0.9953	0.9948	4.5284
Hixon Crowell	0.9923	0.9923	4.2160

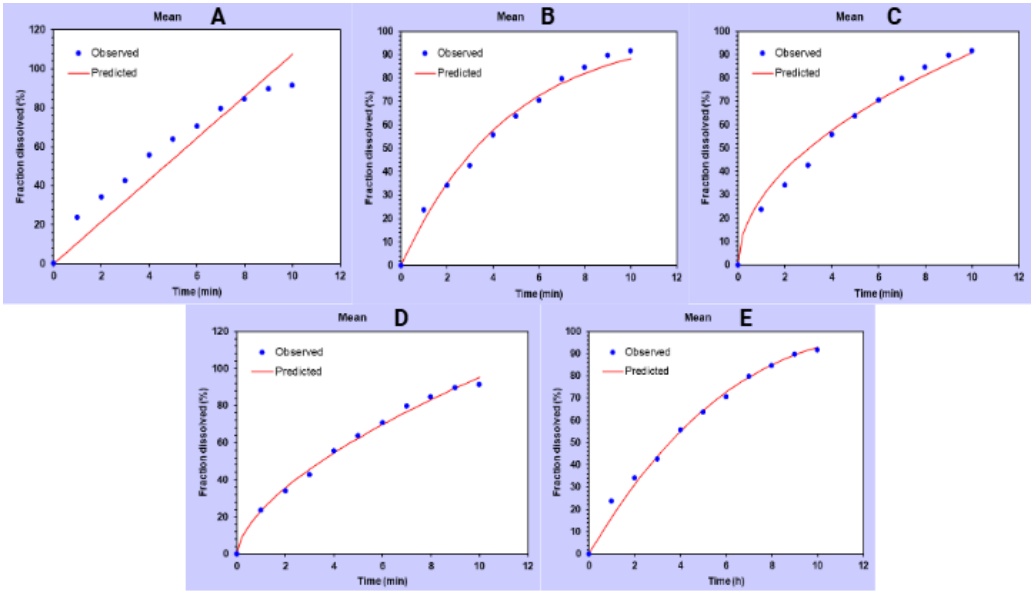

Figure 9: kinetic modeling study (A) Zero order kinetics (B) First order kinetics (C) Higuchi kinetics (D) Korsmeyer peppas kinetics (E) Hixon crowell kinetics

Similarity Factor (f_2)

Dissolution testing was conducted to ensure batch-to-batch uniformity, support formulation development, and provide insight into the in vitro performance and potential bioavailability of the developed system. The dissolution profiles of the optimized nanoparticle-loaded in situ gel formulation (SS-NPs ISG4) were compared with those of the marketed product SUMINAT 25 (Sun Pharmaceutical Industries Ltd., India) using f_2. The calculated f_2 value was 54.30, exceeding the acceptance criterion of 50 and indicating comparable drug-release behavior between the test and reference formulations. As shown in Figure 10, the release pattern of sumatriptan succinate from the prepared formulation closely matched that of the marketed product, confirming in vitro equivalence and supporting the suitability of the optimized formulation for further evaluation.

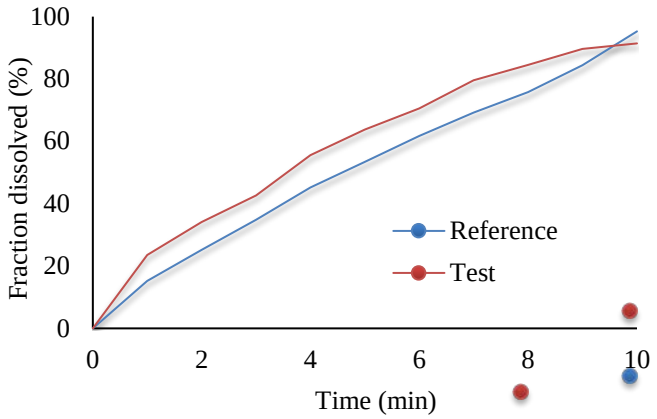

Figure 10: Graph of similarity factor of test formulation (SS-NPs ISG4) and reference formulation (SUMINAT 25)

***Ex vivo* permeation studies**

The ex vivo permeation study used fresh goat nasal mucosa approximately 0.8-1.2 mm thick, including the epithelial layer. To avoid damaging the epithelial surface, the nasal septum and the cartilage below it were carefully taken out with blunt dissection. Before placing the mucosa in the diffusion cell, it was examined to ensure it was even and free of tears. This was done to ensure the barrier remained in place for the 10-hour study. Membranes that were complete and uniform in thickness throughout were chosen. To maintain the tissue alive and hydrated before the experiment, it was also absorbed in synthetic nasal fluid. The absence of unanticipated fluctuations in drug penetration profiles further indicates that the epithelial barrier remained intact throughout the research. The drug release begins with an initial burst during the first hour, indicating rapid diffusion of surface-bound drug. Following this, a steady and nearly linear increase in drug release is observed, suggesting a controlled and sustained release behavior throughout the study period. By the end of 10 hours, 85.24% of the drug is released, showing efficient permeation through the biological membrane, as shown in Figure 11. This release pattern indicates a sustained-release formulation, which is beneficial for maintaining therapeutic drug levels over an extended duration.

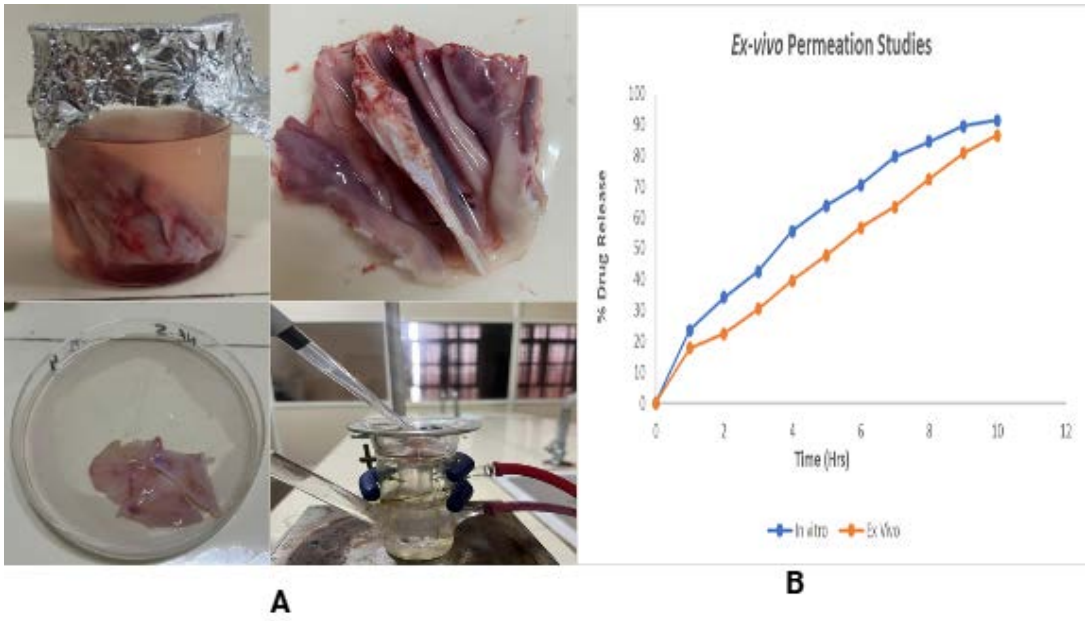

Figure 11: (A) Extraction of goat's nasal mucosal membrane (B) *Ex vivo* and *in vitro* drug permeation study of optimized formulation SS-NPs ISG4

Cell viability and proliferation analysis:

MTT assay

The MTT cell viability experiment was conducted on RPMI-2650 human nasal epithelial cells to assess the cytocompatibility of the blank drug, blank nanoparticles (Blank NPs), and the optimized formulation (SS-NPs ISG4) following 24 hours of exposure. Untreated cells were considered 100% viable, while Triton X-100 (0.1%) served as a positive control for cytotoxicity, showing a significant decrease in viability (~14.44%), thereby validating the test's sensitivity and reliability. A significant concentration-dependent decrease in cell viability was noted for the blank drug. At lower doses (15.62 and 31.25 µg/ml), cell viability was notably high (89.03% and 80.83%, respectively), suggesting little cytotoxicity. However, with increasing concentration, viability gradually decreased, reaching 51.06% at 125 µg/ml and 23.38% at 500 µg/ml. The

determined IC_{50} value of 132.06 µg/ml indicates considerable cytotoxicity at elevated doses, presumably due to direct exposure of cells to unbound drug constituents. On the other hand, blank nanoparticles (Blank NPs) showed enhanced cytocompatibility at all tested doses. Cell viability exceeded 90% at lower dosages (15.62–31.25 µg/ml) and decreased progressively with higher concentrations. At 125 µg/ml, viability was 61.70%, and at 250 µg/ml, it exceeded 50%. The IC_{50} value of 264.27 µg/ml, approximately twice that of the blank drug, indicates that the nanoparticle formulation significantly reduces harmful effects. This enhancement may be related to the polymeric or carrier matrix, which presumably reduces direct cellular exposure and interactions with nasal epithelial cells. The SS-NPs ISG4 formulation exhibited a unique cytotoxicity profile. At reduced doses (15.62–62.5 µg/ml), high cell viability (>79%) was preserved, signifying satisfactory biocompatibility. A more pronounced decrease in viability was noted beyond 125 µg/ml, with cell survival decreasing to 51.96% at 125 µg/ml and to 18.39% at 500 µg/ml. The IC_{50} value of 152.76 µg/ml indicates that SS-NPs ISG4 exhibit more cytotoxicity than blank nanoparticles; however, they remain less toxic than the free drug at comparable quantities, as shown in Table 8. The increased cytotoxicity at higher doses may correlate with the presence of the active ISG4 component, which promotes cellular interactions and biological activity. The MTT assay results showed that all examined formulations exhibited dose-dependent cytotoxicity against RPMI-2650 nasal epithelial cells. Among them, blank nanoparticles exhibited superior nasal compatibility, as indicated by the highest IC_{50} value and by their ability to maintain cell viability across an extensive concentration range. The SS-NPs ISG4 formulation demonstrated satisfactory biocompatibility at low and moderate doses, indicating its appropriateness for nasal administration within a safe therapeutic range.

However, the blank drug exhibited significantly more cytotoxicity, underscoring the benefits of nanoparticle-based systems in enhancing nasal epithelial compatibility. These findings collectively support the use of nanoparticle formulations, specifically SS-NPs ISG4, at optimal doses as promising, comparatively safe vehicles for intranasal drug delivery. Figure 12 (A) shows concentration-dependent cell viability of blank drug, blank nanoparticles, and SS-NPs ISG4, and (B) shows phase contrast microscopic images showing concentration-dependent morphological changes in RPMI-2650.

Table 8: MTT Assay-Summary of Blank drug, Blank NPs, and SS-NPs ISG4 formulation vs RPMI-2650

Treatment Condition	% Cell Viability		
	Blank Drug	**Blank NP's**	**SS-NPs ISG4 formulation**
Untreated	100		
Triton-x 100 0.1%	14.44	14.44	14.44
Blank drug -15.62ug	89.03	97.17	96.16
Blank drug -31.25ug	80.83	90.63	93.09
Blank drug -62.5ug	65.76	71.55	79.62
Blank drug -125ug	51.06	61.70	51.96
Blank drug -250ug	37.15	52.81	39.14
Blank drug -500ug	23.38	38.64	18.39
IC_{50} conc (uG/ml)	132.06 µg/ml	264.27 µg/ml	152.76 µg/ml

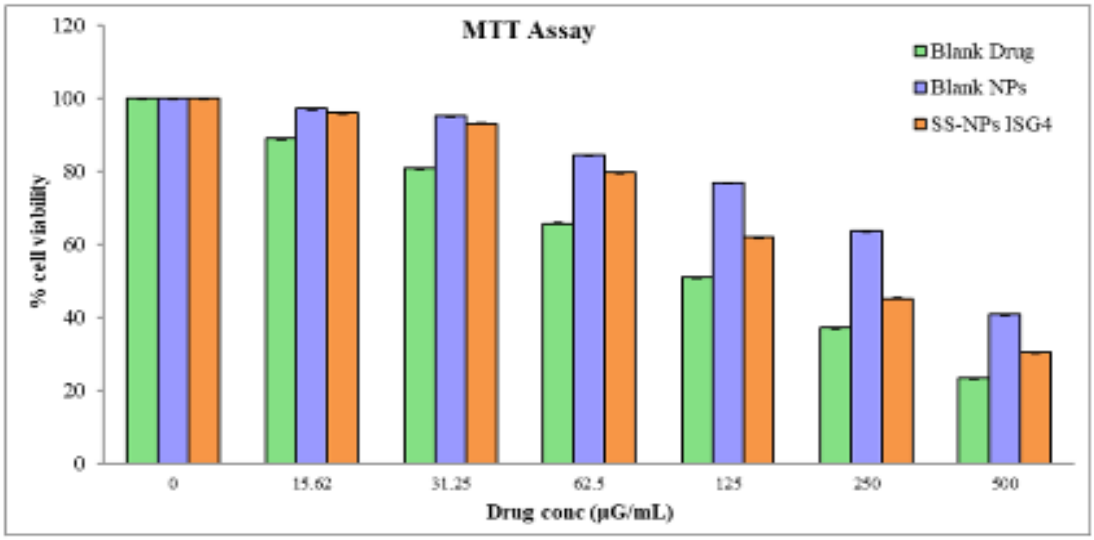

A

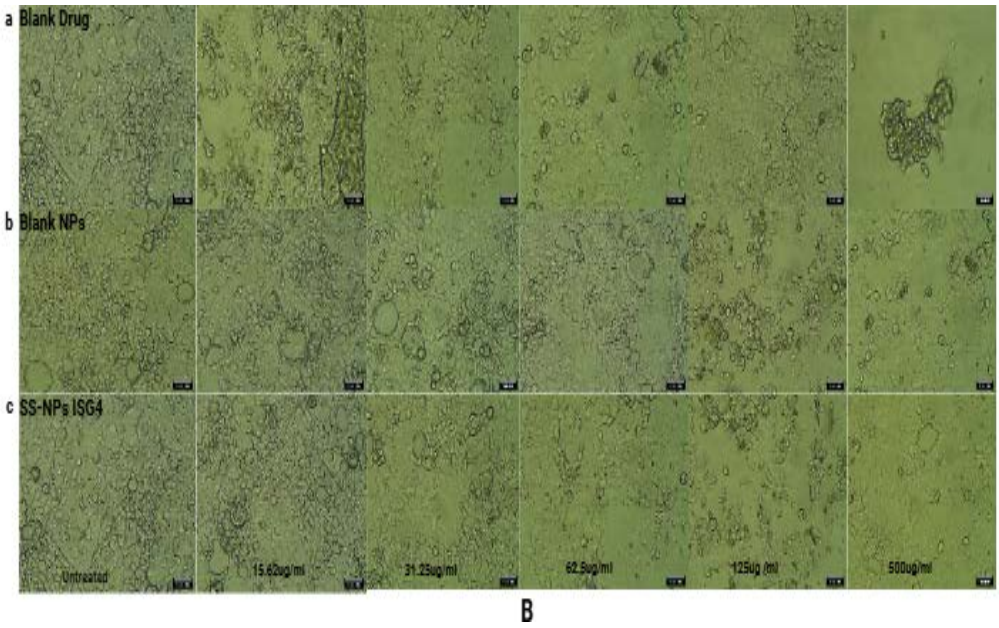

Figure 12: (A) MTT assay showing concentration-dependent cell viability of blank drug, blank nanoparticles, and SS-NPs ISG4 (B) Phase contrast microscopic images showing concentration-dependent morphological changes in RPMI-2650 cells following treatment with a. Blank drug, b. Blank NPs, c. SS-NPs-ISG4 (optimized formulation)

Histopathology Study

The histopathological analysis of the nasal mucosa was conducted to evaluate the potential mucosal toxicity and biocompatibility of the developed formulations following intranasal administration. Figure 13(a) shows the normal nasal membrane with well-preserved pseudostratified columnar epithelium and an intact epithelial lining, with no signs of necrosis, edema, or inflammatory cell infiltration, indicating healthy tissue architecture. In contrast, Figure (b), corresponding to tissue exposed to isopropyl alcohol, revealed significant epithelial damage, detachment of the epithelial layer, and evidence of tissue disruption, confirming the irritant and damaging nature of isopropyl alcohol on the nasal mucosa. Figure (c), representing the group treated with the plain drug solution, showed mild epithelial alterations, including slight lifting and limited cellular disorganization. Notably, Figure (d), which corresponds to the nasal tissue treated with chitosan nanoparticles (Cs-NPs) loaded *in situ* gel, displayed well-maintained epithelial integrity and organized tissue structure with minimal or no histological signs of toxicity or irritation. This indicates that the Cs-NPs-based *in situ* gel formulation is biocompatible and safe for nasal application. Overall, the results demonstrate that the developed nanoparticle-loaded *in situ* gel causes minimal mucosal irritation compared to the drug solution and isopropyl alcohol, highlighting its potential as a safe intranasal drug delivery system.

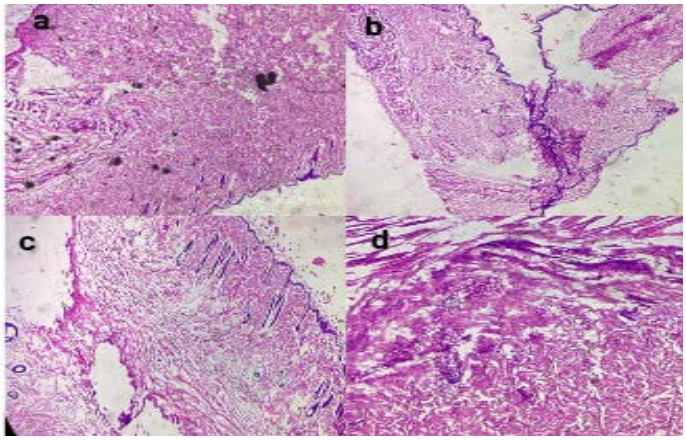

Figure 13: (a) Nasal membrane (b) Isopropyl alcohol (c) Drug Solution (d) Cs-NPs loaded In-situ gel

Stability Studies

Stability studies are crucial for assessing the durability of nanoparticle-based nasal *in situ* gel compositions used for migraine treatment. The physicochemical stability of the proposed formulation was evaluated over 60 days under long-term (25 ± 2 °C) and accelerated (40 ± 2 °C) storage conditions by measuring particle size, PDI, and EE, as shown in Table 9. There were very small changes in particle size and PDI after long-term storage, which shows that the nanoparticles were well-stabilized in the in-situ gel matrix. The particle size remained below 200 nm, and the PDI values remained below 0.35, indicating that the nanoparticle dispersion was still

homogeneous, making it safe for nasal use. These results indicate little aggregation or instability during storage. The effectiveness of entrapment exhibited a small, steady drop over time. This might be because the drug did not spread as widely or because the polymer relaxed. But the numbers stayed within acceptable ranges, which meant that the drug was being held onto well and the formulation was staying stable. On the other hand, faster storage conditions caused the particle size and PDI to increase more rapidly, and the EE to decrease more noticeably. These changes are probably caused by the molecules moving about more, and the drug-polymer interactions become weaker as the temperature and humidity rise. Still, the observed changes remained below permissible limits, indicating they were caused by stress rather than by the instability of the formulation. The stability findings show that the nanoparticle-loaded nasal *in situ* gel has good physicochemical stability when stored for a long time and works well when circumstances quickly change. This means it is good for delivering drugs via the nose to help with migraines.

Table 9: Stability Evaluation Parameters

Time (Days)	Particle Size (nm)		PDI		Entrapment Efficiency (%)	
	At 25°C	At 40 °C	At 25°C	At 40 °C	At 25°C	At 40 °C
0	154.3 ± 5.2	155.4 ± 5.2	0.348 ± 0.02	0.349 ± 0.02	85.6 ± 1.4	82.6 ± 1.4
15	170.1 ± 4.8	174.6 ± 5.9	0.318 ± 0.02	0.328 ± 0.03	81.9 ± 1.3	80.9 ± 1.6
30	172.6 ± 5.0	181.2 ± 6.4	0.325 ± 0.03	0.346 ± 0.03	81.1 ± 1.5	78.6 ± 1.8
45	175.8 ± 5.6	189.5 ± 7.1	0.331 ± 0.03	0.338 ± 0.04	80.4 ± 1.6	75.9 ± 2.0
60	178.9 ± 6.1	198.3 ± 7.8	0.238 ± 0.03	0.291 ± 0.04	79.8 ± 1.7	73.4 ± 2.2

DISCUSSION

The distribution of drugs to the brain for the treatment of neurological conditions presents significant challenges due to biological barriers, such as the BBB, and the distinctive features of drug molecules, including molecular weight and hydrophilicity or hydrophobicity. Scientists have made several efforts to improve drug delivery to the brain via the BBB. The literature indicates that several studies have explored alternative, viable, and practicable methods of drug administration compared with current techniques. One method involves the delivery of drugs through the nasal route, bypassing the BBB. The study presents the development of sumatriptan succinate-loaded chitosan nanoparticles via ionic gelation, and the optimized SS-NPs were further incorporated into the prepared in situ gel by the cold method using Poloxamer 407 (18% w/v), HPMC K100 (0.5% w/v), and Carbopol 934 (0.5% w/v).

The Box-Behnken design was used to optimize SS-NPs, with chitosan, poloxamer, and STPP as independent variables and EE%, DL%, and DR% as dependent variables. Polynomial equations were formulated using the BBD to study the findings, revealing that an increase in chitosan concentration was associated with a decrease in EE, possibly due to excessive viscosity or particle aggregation, whereas increased concentrations of poloxamer and STPP significantly enhance entrapment efficiency due to more effective crosslinking and particle stabilization. The quadratic terms suggest that increasing chitosan concentration beyond an ideal value could reduce DL, likely due to increased polymer entrapment capability once a certain threshold is exceeded. Poloxamer and TPP have negative quadratic effects, indicating that increasing these factors beyond acceptable thresholds reduces DL efficiency, likely due to particle instability or drug expulsion. Polynomial equations indicated that increasing chitosan and STPP concentrations might enhance DR, whereas high poloxamer concentrations could decrease DR, potentially due to excessive gelation or disruption of drug diffusion pathways. The particle size of the developed nanoparticles increased, likely due to the formation of bigger coacervates resulting from the increased polymer concentration.

The optimized SS-NPs exhibited a positive surface charge of +22.79 mV, due to the presence of protonated amine groups on their surface. The increased positive charge maintained colloidal stability and facilitated electrostatic contact with the negatively charged nasal mucosa, hence improving muco-adhesion and drug absorption.

The developed drug nanoparticle-loaded in situ gel (SS-NPs ISG4) showed a desirable balance of physicochemical, rheological, and biopharmaceutical characteristics appropriate for nasal administration. The formulation showed low viscosity in the sol state (48 cps), facilitating administration, and a significant rise in viscosity upon gelation (589 cps), which is beneficial for extended nasal retention and reduced mucociliary clearance. The sol–gel transition behavior is predominantly

influenced by Poloxamer 407, whereas HPMC K100 and Carbopol 934 synergistically improve viscosity via polymer hydration and network formation. The drug content (95.82%) and entrapment efficiency (82.76%) showed effective drug retention and homogeneous distribution inside the nanoparticle-loaded gel matrix.

The use of secondary polymers likely increased concentration and limited drug diffusion during formulation, thereby reducing drug loss. The formulation exhibited an ideal gelation temperature of 32–33 °C, validating its thermoresponsive nature and compatibility with in situ gel formation at nasal cavity temperature. These characteristics ensure that the formulation remains in a sol state throughout administration and swiftly converts into a gel upon contact with the nasal mucosa. In vitro drug release experiments showed significant cumulative drug release (90.41%), suggesting controlled and sustained release behavior. This can be related to the effective diffusion barrier created by the nanoparticulate system and the hydrated polymeric gel network. Moreover, the formulation exhibited improved ex vivo penetration (88.64%), presumably due to increased mucosal contact, optimized viscosity, and the addition of polymers that promote drug diffusion across the nasal membrane.

The ex vivo and in vitro release studies use Simulated Nasal Fluid (SNF) at pH 6.8, aligning with the specified pH of the formulated gel (6.8 ± 0.1). The usual pH of the nose is between 5.5 and 6.5, although it can shift toward neutral under certain conditions, due to irritation, or as a result of buffering effects from the formulation. A pH of 6.8 was chosen to ensure that the formulation and the release medium were compatible. This ensured that the assessment was always the same and could be repeated. Carbopol also changes size depending on pH. When the pH is close to neutral, it ionizes more and makes the polymer less stiff. Studies conducted at pH 6.8 are slightly higher than normal but still safe for the body. This amount of acid helps the gel swell and release the drug without damaging the nose. So, the chosen pH strikes an excellent balance among being physiologically relevant, maintaining formulation stability, and ensuring consistent release performance. The kinetic analysis showed the Korsmeyer–Peppas model provided the best fit, as evidenced by the lowest SSR value (41.3131), highest R^2 (0.9953), and adjusted R^2 (0.9948), and a similarity factor value of 54.30, exceeding the acceptance criterion of 50, thereby indicating comparable drug release behavior between the test and reference formulations. Histopathology results demonstrate that the developed nanoparticle-loaded *in situ* gel causes minimal mucosal irritation compared to the drug solution and isopropyl alcohol, highlighting its potential as a safe intranasal drug delivery system. Furthermore, the MTT study showed a concentration-dependent decline in cell viability across all samples studied. The SS-NPs ISG4 formulation exhibited higher cell viability than the blank drug at the same doses, indicating reduced cytotoxicity due to nanoparticle encapsulation. Blank nanoparticles exhibited the highest cell viability across all concentrations, thereby supporting the biocompatibility of the carrier system. The findings indicate that SS-NPs ISG4 exhibit cytocompatibility at reduced doses and are safer than the free drug, thereby supporting their suitability for nasal administration. The stability findings indicate that the nanoparticle-loaded nasal in situ gel exhibits good physicochemical stability during extended storage.

CONCLUSION

Drugs can be administered directly to the brain via the nasal route. The medication is administered via the nose as snuff, spray, or a nebulized solution, enabling it to pass through the nasal mucous membrane and into the bloodstream. On the other hand, it can quickly remove the medication through the nasal cavity. A unilateral, pounding headache is the hallmark of migraine, a nervous system disorder. Physical activity, light, sound, or Odors can all aggravate migraines, which can last anywhere from four hours to several days. Regular use of migraine medicine may have serious side effects in addition to symptoms. The oral absorption of migraine medications is quite low. Parenterally administered medications accumulate in higher concentrations in other organs and show insufficient transport to the site of action (the brain), resulting in serious side effects. Consequently, developing a method that delivers the medication at sufficiently high concentrations to produce a therapeutic effect is crucial. Migraine remains a highly prevalent and disabling neurological disorder that demands rapid and effective therapeutic intervention. Conventional oral and parenteral antimigraine therapies are often limited by delayed onset of action, poor patient compliance, extensive first-pass metabolism, and restricted drug transport across the blood–brain barrier. In this context, intranasal drug delivery has gained increasing attention as a non-invasive route that enables rapid systemic absorption and direct nose-to-brain transport.

The present study is significant because it integrates nanoparticle-based drug delivery with a mucoadhesive, thermo-responsive in situ nasal gel to overcome critical physiological and formulation challenges associated with nasal administration. Nanoparticle encapsulation enhances drug stability, bioavailability, and brain targeting, while the thermo-responsive mucoadhesive gel improves nasal residence time, minimizes mucociliary clearance, and provides controlled drug release. This synergistic approach directly addresses the unmet need for fast-acting, efficient brain-delivery systems in acute migraine management. Furthermore, the development and detailed characterization of this platform hold strong translational relevance in today's pharmaceutical landscape, where patient-centric, non-invasive, and targeted therapies are increasingly prioritized. By demonstrating the potential for rapid onset of action, reduced systemic side effects, and improved therapeutic outcomes, this study advances next-generation nose-to-brain drug delivery strategies for migraine and other central nervous system disorders.

The prepared nanoparticle-loaded mucoadhesive in situ nasal gel showed significantly better ex vivo penetration across goat nasal mucosa than the control formulation. However, this study did not find any direct indication of brain targeting. The observed increase in permeability suggests that nose-to-brain delivery could be improved, but additional in vivo pharmacokinetic and biodistribution studies are needed to confirm improved brain targeting. Consequently, the assertion of "enhanced brain delivery" is to be regarded as a predicted result derived from permeation studies rather than a definitively established impact.

Future Prospects

To verify its translational utility, future research should focus on a thorough in vivo evaluation of the developed mucoadhesive nanoparticle-loaded thermo-responsive in situ nasal gel. To validate enhanced brain targeting via the olfactory and trigeminal pathways, thorough pharmacokinetic and biodistribution investigations in suitable animal models are required. The relationship between cerebral medication concentrations and therapeutic effects will be clarified by pharmacodynamic efficacy studies using established migraine models. Additionally, evaluations of ciliotoxicity, repeated-dose toxicity, and long-term nasal safety are important in determining tolerance. To support the clinical translation and regulatory approval of this potential intranasal delivery method, the feasibility of scaling up and device compatibility should also be assessed.

FINANCIAL ASSISTANCE

NIL

CONFLICT OF INTEREST

The authors declare no conflict of interest.

AUTHOR CONTRIBUTION

Mansi Butola contributed to data collection and writing of the manuscript. Vikash Jakhmola contributed to conceptualization, editing, and critical review of the manuscript. Both authors reviewed and approved the final version of the manuscript.

REFERENCES

[1] Torres J, Silva R, Farias G, Lobo JMS, Ferreira DC, Silva AC, et al. Enhancing acute migraine treatment: Exploring solid lipid nanoparticles and nanostructured lipid carriers for the nose-to-brain route. *Pharmaceutics*, **16**, 1297 (2024) https://doi.org/10.3390/pharmaceutics16101297

[2] Yadav RK, Shah K, Dewangan HK. Intranasal drug delivery of sumatriptan succinate-loaded polymeric solid lipid nanoparticles for brain targeting. *Drug Dev. Ind. Pharm.*, **48**, 21–28 (2022) https://doi.org/10.1080/03639045.2022.2090575

[3] Nerella N, Vasudha B. Design, development, and optimization of sumatriptan loaded ethosomal intra-nasal nanogel for brain targeting. *Journal of Applied Pharmaceutical Research*, **12**, 83–98 (2024) https://doi.org/10.69857/joapr.v12i4.610

[4] Alshraim A, Alshora D, Ashri L, Alhusaini A, Alanazi N, Safwan NM. In situ thermosensitive mucoadhesive nasal gel containing sumatriptan: In vitro and ex vivo evaluations. *Polymers (Basel)*, **16**, 3422 (2024) https://doi.org/10.3390/polym16233422

[5] Assadpour S, Shiran MR, Asadi P, Akhtari J, Sahebkar A. Harnessing intranasal delivery systems of sumatriptan for the treatment of migraine. *Biomed Res. Int.*, 1–14 (2022) https://doi.org/10.1155/2022/xxxxxxx

[6] Mathure D, Sutar AD, Ranpise H, Pawar A, Awasthi R. Preparation and optimization of liposome containing thermosensitive in situ nasal hydrogel system for brain delivery of sumatriptan succinate. *Assay Drug Dev. Technol.*, **21**, 3–16 (2023) https://doi.org/10.1089/adt.2022.088

[7] Mathure D, Ranpise H, Awasthi R, Pawar A. Formulation and characterization of nanostructured lipid carriers of rizatriptan benzoate-loaded in situ nasal gel for brain targeting. *Assay Drug Dev. Technol.*, **20**, 211–224 (2022) https://doi.org/10.1089/adt.2022.044

[8] Kalita R, Sarma A, Baruah H, Zaman A, Goswami D. Nose-to-brain delivery of curcumin loaded therapeutic nanostructures for

neurodegenerative diseases. *Biopharm. Drug Dispos.* (2026) https://doi.org/10.1002/bdd.70021

[9] Butola M, Nainwal N. Non-invasive techniques of nose to brain delivery using nanoparticulate carriers: Hopes and hurdles. *AAPS PharmSciTech*, **25**, 256 (2024) https://doi.org/10.1208/s12249-024-02946-z

[10] Barangule SP, Maru AD. Design and development of thermosensitive rectal in situ gel from *Luffa acutangula* fruits for the treatment of ulcerative colitis. *Journal of Applied Pharmaceutical Research*, **12**, 102–115 (2024) https://doi.org/10.69857/joapr.v12i5.761

[11] Mankar SD, Andhale A, Siddheshwar SS, Mhaske MP. Emodin-loaded mucoadhesive in situ nasal gel: Design, optimization, and evaluation for migraine therapy. *BioNanoScience*, **15**, 412–421 (2025) https://doi.org/10.1007/s12668-025-02035-w

[12] Dudhat K, Kachhadiya Y, Chotaliya M. Development of a thermosensitive in-situ nasal gel of teriflunomide for targeted CNS delivery in multiple sclerosis. *J. Pharm. Innov.*, **21**, 47–58 (2025) https://doi.org/10.1007/s12247-025-10291-2

[13] Mujtaba MA, Rashid MA, Godbole MD, Alhamhoom Y, Shende DS, Alshehri S, et al. Escitalopram oxalate-loaded chitosan nanoparticle in situ gel intended for direct nose-to-brain delivery: In vitro, ex vivo, and in vivo pharmacokinetic evaluation. *Front. Pharmacol.*, **16**, 1577331 (2025) https://doi.org/10.3389/fphar.2025.157733

[14] Rawat PS, Ravi PR, Mahajan RR. Design, pharmacokinetic, and pharmacodynamic evaluation of a lecithin-chitosan hybrid nanoparticle-loaded dual-responsive in situ gel of nebivolol for effective treatment of glaucoma. *Discover Nano*, **19**, 156 (2024) https://doi.org/10.1186/s11671-024-04109-2

[15] Hussain S, Malik N, Tulain U, Erum A, Mahmood A, Akram S, et al. Itraconazole-loaded polycaprolactone nanoparticle gel for enhanced transdermal delivery: Development, characterization, and ex vivo evaluation. *Int. J. Nanomedicine*, **20**, 15655–15681 (2025) https://doi.org/10.2147/IJN.S56074

[16] Bhute H, Salve PS, Sheikh S, Hussain UM, Tammewar S, Tatode AA, et al. Development of a gellan–Carbopol in situ gel system for intranasal delivery of artemether-loaded SLNs: Optimization and kinetic evaluation. *J. Pharm. Innov.*, **21**, 73–84 (2025) https://doi.org/10.1007/s12247-025-10263-6

[17] Bajwa M, Tabassam N, Hameed H, Irfan A, Zaman M, Khan MA, et al. Thermo-responsive sol–gel-based nano-carriers containing terbinafine HCl: Formulation, in vitro and ex vivo characterization, and antifungal activity. *Gels*, **9**, 830 (2023) https://doi.org/10.3390/gels9100830

[18] Islam MM, Kumar M, Mujtaba MA, Elhassan GO, Abdoun S, Misbah M, et al. Formulation development, Box–Behnken design-based optimization and evaluation of cisplatin-loaded chitosan nanoparticles embedded in mucoadhesive buccal film for targeted oral cancer therapy. *J. Pharm. Innov.*, **20**, 276–289 (2025) https://doi.org/10.1007/s12247-025-10163-9

[19] Longo E, Giuliano E, Gagliardi A, Gaetano V, Frisina M, Verdiglione M, et al. In situ forming poloxamer-based thermo-sensitive hydrogels for ocular application: A focus on the derivatives 407 and 188. *Gels*, **11**, 752 (2025) https://doi.org/10.3390/gels11090752

[20] Deshmane S, Chavan V, Nagpure S, Jain S, Solanki H, Sarode R, et al. Quality by design optimization of zolmitriptan nanostructured lipid carriers for nose-to-brain delivery in migraine. *BioNanoScience*, **16**, 3–15 (2025) https://doi.org/10.1007/s12668-025-02278-7

[21] Jha B, Majie A, Roy K, Lim WM, Gorain B. Glycyrrhizic acid-loaded poloxamer and HPMC-based in situ forming gel of acacia honey for improved wound dressing: Formulation optimization and characterization for wound treatment. *ACS Appl. Bio Mater.*, **8**, 310–328 (2024) https://doi.org/10.1021/acsabm.4c01212

[22] Omidi M, Saeedi M, Zahiri MA, Azimi S, Mohammadian E, Hashemi SMH. Green arbutin–chitosan nanoparticles gel as an eco-friendly and promising product for skin lightening: In vitro and in vivo assessment. *Nanomed. J.*, **13**, 224–235 (2026) https://doi.org/10.22038/NMJ.2025.83053.2075

[23] Wang Y, Han Z, Zhang C, Kang X, Jiang T, Li R, et al. Curcumin extraction and preparation and optimization of curcumin nanoparticles. *Chin. J. Tissue Eng. Res.*, **30**, 362–368 (2026) https://doi.org/10.12307/2025.497

[24] Sarkar P, Desavathu M, Jain S, Mishra AK, Reddy RS, Sah PK. Mucoadhesive polymeric nanoparticles of fexofenadine hydrochloride for ocular delivery: Formulation, characterisation, and enhanced permeation studies. *J. Pharm. Innov.*, **21**, 65–77 (2025) https://doi.org/10.1007/s12247-025-10296-x

[25] Suhagiya K, Borkhataria CH, Gohil S, Manek RA, Patel KA, Patel NK, et al. Development of mucoadhesive in situ nasal gel formulation for enhanced bioavailability and efficacy of rizatriptan in migraine treatment. *Results Chem.*, **6**, 101010 (2023) https://doi.org/10.1016/j.rechem.2023.101010

[26] Mathure D, Ranpise H, Awasthi R, Pawar A. Formulation and characterization of nanostructured lipid carriers of rizatriptan benzoate-loaded in situ nasal gel for brain targeting. *Assay Drug Dev. Technol.*, **20**, 211–224 (2022) https://doi.org/10.1089/adt.2022.044

[27] Adwan S, Obeidi T, Al-Akayleh F, et al. Chitosan nanoparticles embedded in in situ gel for nasal delivery of imipramine hydrochloride: Short-term stage development and controlled release evaluation. *Polymers*, **16**, 3062 (2024) https://doi.org/10.3390/polym16213062

[28] Patil VL, Rane BR, Mane NP, Jain AS. Preparation and optimization of beta-sitosterol nanosuspension-loaded in situ gel using Box–Behnken model for the treatment of prostate cancer.

Micro Nanosyst., **17**, 27–44 (2024) https://doi.org/10.2174/0118764029328588240816075844

[29] Bilapatte A, More A, Satpute K, Syed SM. Formulation and evaluation of carbamazepine loaded ethosomal nasal in situ gel for brain targeted drug delivery. *J. Holist. Integr. Pharm.*, **6**, 57–63 (2025)

[30] Rahbar N, Darvish S, Farrahi F, Kouchak M. Chitosan/carbomer nanoparticles-laden in situ gel for improved ocular delivery of timolol: In vitro, in vivo, and ex vivo study. *Drug Deliv. Transl. Res.*, **15**, 1210–1220 (2024) https://doi.org/10.1007/s13346-024-01663-1

[31] Mandal S, Das NR, Mukherjee K, Giri TK. In vitro, ex vivo, and in vivo evaluation of polysaccharide-based thermo-sensitive in situ gel for the treatment of glaucoma. *J. Biomater. Appl.*, **40**, 650–665 (2026) https://doi.org/10.1177/08853282251369232

[32] Rahmatpanahi A, Bavali A, Farhadi M, Bagheri-Khoulenjani S, Kaviani-Samani S. Illuminating RPMI-1640: Fluorescence dynamics and optical insights for biological applications. *J. Photochem. Photobiol. A Chem.*, **469**, 116537 (2025) https://doi.org/10.1016/j.jphotochem.2025.116537

[33] Butola M, Nainwal N. In vivo, in vitro, and ex vivo experimental models for nose-to-brain drug delivery. *Drug Deliv. Lett.*, **15** (2025) https://doi.org/10.2174/0122103031378584250829054818

[34] Yadav R, Mani RJ, Sharma A, Kumar A, Katare D. Formulation and optimization of metformin-berberine loaded solid lipid nanoparticles for their neuroprotective effects in the brain. *Journal of Applied Pharmaceutical Research*, **13**, 114–133 (2025) https://doi.org/10.69857/joapr.v13i5.1356

[35] Steyn JD, Haasbroek-Pheiffer A, Pheiffer W, Weyers M, van Niekerk SE, Hamman JH, et al. Evaluation of drug permeation enhancement by using in vitro and ex vivo models. *Pharmaceuticals*, **18**, 195 (2025) https://doi.org/10.3390/ph18020195

[36] Das B, Umashankar MS. Design and optimization of a mucoadhesive gel containing solid lipid nanoparticles for sublingual and nasal delivery of a low bioavailable drug. *Preprints.org* (2025)

[37] Gattani V, Dawre S. Development of favipiravir-loaded PLGA nanoparticles entrapped in in situ gel for treatment of COVID-19 via nasal route. *J. Drug Deliv. Sci. Technol.*, **79**, 104082 (2023) https://doi.org/10.1016/j.jddst.2022.104082

[38] Jabir SA, Rajab N. Preparation, in vitro, ex vivo, and pharmacokinetic study of lasmiditan as intranasal nano-emulsion-based in situ gel. *Pharm. Nanotechnol.*, **13**, 239–253 (2024) https://doi.org/10.2174/0122117385285009231222072303